The Amide Rotational Barrier in Isonicotinamide: Dynamic NMR and Ab Initio Studies

Garett M. Leskowitz,[†] Nima Ghaderi,[†] Ryan A. Olsen,[†] Kari Pederson,[‡] Mary E. Hatcher,[§] and Leonard J. Mueller*,[†]

Department of Chemistry, University of California, Riverside, California 92521, Scripps College, Claremont, California 91711, and W. M. Keck Science Center, The Claremont Colleges, Claremont, California 91711

Received: August 31, 2004; In Final Form: October 1, 2004

We report use of dynamic nuclear magnetic resonance (NMR) to measure the amide rotational barrier in isonicotinamide. A significant challenge to obtaining good transition rates from dynamic NMR data is suppression of errors due to inherent line widths associated with transverse relaxation. We address this challenge with a fitting procedure that incorporates transverse relaxation over the temperature range of interest simply and reliably. The fitting model is nonlinear in only one of the fit parameters, namely, the activation enthalpy. This reduces parameter estimation to solution of a single transcendental equation, which avoids both a fine search over a multidimensional parameter space and extrapolation of a "limiting line width" solely from slow-exchange data. The activation enthalpy $\Delta H^{\ddagger}$ measured for isonicotinamide, $+14.1 \pm 0.2$ kcal/mol, falls between those of its regioisomers picolinamide and nicotinamide, which were reported in an earlier study. In that study, ab initio calculations of the rotational barriers helped to discern the relative importance of steric, electronic, and hydrogen-bonding effects in this biochemically significant combination of pyridine-ring and carboxamide moieties. A direct comparison between isonicotinamide and nicotinamide, where steric and hydrogen-bonding effects differ only slightly, permits a closer study of electronic considerations.

Introduction

Amide bonds play a critical role in chemistry and biology, and their rotational potentials are fundamental in determining structure and dynamics in small molecules as well as in large molecules such as proteins and nucleic acids. An important aspect of the amide linkage is the partial double bond character that results from donation of lone-pair electron density from the amide nitrogen to the carbonyl carbon. This leads to a significantly higher barrier to C−N bond rotation than those found in other amines. This barrier can be modified by a number of structural and electronic properties and has attracted significant experimental and theoretical interest.[1−18] Recently, we reported amide bond rotational barriers for the regioisomers picolinamide (2-pyridinylcarboxamide) and nicotinamide (3-pyridinylcarboxamide, vitamin B_3) (Scheme 1) as determined by dynamic NMR spectroscopy.[19] These two medicinally significant pyridine carboxamides showed a substantial difference of 5.4 kcal/mol in their enthalpies of activation. Ab initio calculations of the rotational barriers were in good agreement with the experimentally determined values and helped partition this enthalpy difference into three major contributions. Of principal importance was a difference in steric interactions in the ground states of picolinamide and nicotinamide, superior π electron donation from the pyridine ring in the transition state of nicotinamide, and an intramolecular hydrogen bond in the ground state of picolinamide. Here, we report the rotational barrier for the third and final regioisomer, isonicotinamide (4-pyridinylcarboxamide, Scheme 1). Isonicotinamide's barrier ($\Delta H^{\ddagger} = +14.1 \pm 0.2$ kcal/mol) is somewhat greater than that of nicotinamide ($+13.1 \pm 0.3$ kcal/mol), primarily due to reduced resonance stabilization of its transition-state structure compared to nicotinamide's, but it is not so large as picolinamide's ($+17.9 \pm 0.4$ kcal/mol). Ab initio calculations of the rotational barriers again agree well with the experimentally determined values and offer unique insight into the pyridine ring electronic structure.

SCHEME 1: The Pyridine Carboxamides

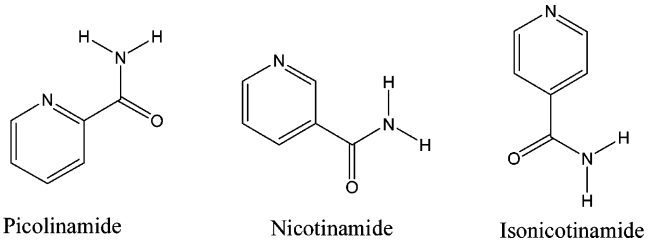

As part of the data analysis, we introduce a new least-squares fitting procedure for extracting the enthalpy and entropy of activation from dynamic NMR data that avoids imposing a "limiting line width" measured experimentally under conditions of negligible exchange. It is well-known[20−22] that an error in the limiting line width estimate effectively contributes a constant offset to the extracted rate in slow exchange. Such an error might arise because the T_2 in slow exchange is poorly representative of the T_2 over the full observed temperature range due to temperature-dependent association between molecules or merely because the value is an extrapolation from a small number of data points. This error is avoided in our analysis by fitting an apparent rate versus temperature profile to a composite curve that includes a constant term for the limiting line width plus the temperature-weighted exponential rise of transition state theory. To fit the composite curve robustly, we adapt the elegant but somewhat underutilized method of Jeričević et al.[23] and linearize the part of the fitting procedure used to extract the

* To whom correspondence should be sent. E-mail: Leonard.Mueller@ucr.edu.
[†] Department of Chemistry, University of California.
[‡] Scripps College.
[§] W. M. Keck Science Center, The Claremont Colleges.

10.1021/jp0460689 CCC: $30.25
Published on Web 01/25/2005

T_2-dependent contribution to the line width and the transition-state entropy. Under these conditions, convergence to the global optimum for the line width and entropy can be guaranteed, while determining the best-fit enthalpy is reduced to solving a single transcendental equation. We find better convergence for this method than for standard nonlinear least-squares procedures, which in some cases repeatedly failed to find a globally minimal χ^2 statistic. In this model, we are explicitly assuming that the limiting line width remains constant over the entire temperature range, although this model can easily be extended to situations in which $1/T_2$ has a linear or even polynomial temperature dependence.

Theory and Data Analysis. We begin with a brief summary of the effects of chemical exchange on the NMR line shape. We describe only equivalent or mutual exchange, where the two exchanging molecular states are isoenergetic, as is the case for amide proton exchange under C−N bond rotation. The analysis follows closely the work of Bain and co-workers[24,25] and of other canonical references.[20,26] Let $\mathbf{m}(t)$ denote the complex column vector

$$\begin{pmatrix} m_{a-}(t) \\ m_{b-}(t) \end{pmatrix} \tag{1}$$

where $m_{j-}(t) = m_{jx}(t) - im_{jy}(t)$ denotes transverse magnetization at site $j \in \{a,b\}$ at time t. In the simplest two-site exchange model, we neglect couplings to other nuclei, and the equation of motion for $\mathbf{m}(t)$ is $d\mathbf{m}/dt = \mathbf{M}\cdot\mathbf{m}(t)$, where

$$\mathbf{M} = \begin{pmatrix} +i\omega_a - 1/T_{2a} - k & k \\ k & +i\omega_b - 1/T_{2b} - k \end{pmatrix} \tag{2}$$

The terms in $\mathbf{M}$ account for precession (at the Larmor frequencies ω_j), for transverse relaxation (with time constants T_{2j}), and for exchange (at rate k). As $\mathbf{M}$ is constant, the solution $\mathbf{m}(t) = e^{\mathbf{M}t}\mathbf{m}(0)$ to the equation of motion is readily obtained by writing $\mathbf{M}$ in its eigenbasis and then exponentiating.

The result is the free induction decay (FID), which is the sum of $\mathbf{m}$'s two components:

$$s(t) = (1,1)\cdot\mathbf{m}(t) = m_{a-}(t) + m_{b-}(t) \tag{3}$$

Given the initial condition $\mathbf{m}(0) = \begin{pmatrix} 1 \\ 1 \end{pmatrix}$ present after a single 90-degree pulse, the result is

$$s(t) = e^{-rt}((1 - ik/\epsilon)e^{i(\sigma+\epsilon)t} + (1 + ik/\epsilon)e^{i(\sigma-\epsilon)t}) \tag{4}$$

where

$$r = k + \frac{1}{T_2} \tag{5}$$

and

$$\epsilon = \sqrt{(\Omega + i\zeta)^2 - k^2} \tag{6}$$

and where

$$\sigma = \frac{1}{2}(\omega_a + \omega_b),\ \Omega = \frac{1}{2}(\omega_a - \omega_b) \tag{7a,b}$$

$$\frac{1}{T_2} = \frac{1}{2}\left(\frac{1}{T_{2a}} + \frac{1}{T_{2b}}\right),\ \text{and}\ \zeta = \frac{1}{2}\left(\frac{1}{T_{2a}} - \frac{1}{T_{2b}}\right) \tag{8a,b}$$

In what follows, we assume that there is no difference in the transverse relaxation times associated with the two sites ($\zeta = 0$). While this simplifies the equations below and is often the case experimentally, it is by no means required. If the exchange rate k is less than Ω (one-half the difference between the angular Larmor frequencies) then ϵ is real, and the signal has two distinct angular frequency components, one at $\sigma + \epsilon$ and one at $\sigma - \epsilon$. This is the slow-exchange regime. (The slow-exchange regime is often more precisely defined by $k < 2^{-1/2}\ \Omega$. When this condition fails, the second derivative of the spectrum's real part with respect to frequency is zero or negative for all values of T_2, and the peaks visually coalesce.) The Fourier transform of the two decaying exponentials in eq 4 is

$$S(\omega) = \frac{1 - ik/\epsilon}{r + i(\omega - (\sigma + \epsilon))} + \frac{1 + ik/\epsilon}{r + i(\omega - (\sigma - \epsilon))} \tag{9}$$

Thus, the slow-exchange spectrum always consists of two Lorentzian lines of equal amplitude. The lines are also characterized by a phase lean, $\phi = \tan^{-1}(k/\epsilon) = \sin^{-1}(k/\Omega)$, with one line's lean equal to the other's but of opposite sign. In fast exchange (where $k > \Omega$), ϵ is purely imaginary. In this case eq 9 still applies, but the two Lorentzians now share the same angular frequency, σ, but differ in width and amplitude. In this work, we fit the NMR data in slow exchange to the real part of $S(\omega)$

$$S_{\mathrm{Re}}(\omega) = \frac{A}{2\pi}\left(\frac{r - k/\epsilon(\omega - (\sigma + \epsilon))}{r^2 + (\omega - (\sigma + \epsilon))^2} + \frac{r + k/\epsilon(\omega - (\sigma - \epsilon))}{r^2 + (\omega - (\sigma - \epsilon))^2}\right) \tag{10}$$

with A denoting the peak area. This approach works as long as the system remains in slow exchange, so that ϵ, when it is real, contributes to the frequency of the peaks but not the width.

The predominant effects of an increase in k are to broaden the NMR lines (through $r(k)$, eq 5) and then to draw them together toward coalescence (through $\epsilon(k)$, eq 6). A further effect of k is to modulate the phase lean ϕ of the Lorentzians as they draw together. Since this phase lean interacts strongly with first-order phase adjustments and quadratic baseline components in the measured spectra, in practice we extract the apparent rate $r = k + 1/T_2$, which is also the half-width of the NMR lines in radians per second, and use it to estimate k. Indeed, the goal in fitting temperature-dependent NMR spectra is to obtain the rate k as a function of temperature T. Thus $k(T_i)$ could be extracted from spectrum i and the results subsequently fit to transition state theory,[24,27] which gives the rate constant at temperature T in terms of the entropy $\Delta S^{\ddagger}$ and enthalpy $\Delta H^{\ddagger}$ of activation:

$$k = \frac{k_B T}{h} e^{+\Delta S^{\ddagger}/R} e^{-\Delta H^{\ddagger}/RT} \tag{11}$$

Here, k_B denotes the Boltzmann constant, h denotes Planck's constant, and R denotes the gas constant.

A significant challenge to obtaining reliable rate estimates from fits to NMR spectra is an "inherent" line width, which is characterized by T_2.[20] In the slow-exchange regime, this contributes an overall constant $1/T_2$ to the half-width r when T_2 is fixed across the experimentally observed temperature interval. A commonly used procedure is to estimate $1/T_2$ in slow exchange, subtract this estimate from the apparent half-widths, and then use the results either directly in a fit to the transition state theory expression or in an Eyring plot of $\ln k/T$ vs $1/T$. This can be problematic, as small errors in the estimated T_2 can exert a strong influence on the best-fit thermodynamic quantities. For example, we have previously reported a case in which, when the slow-exchange T_2 is varied by ±10%,

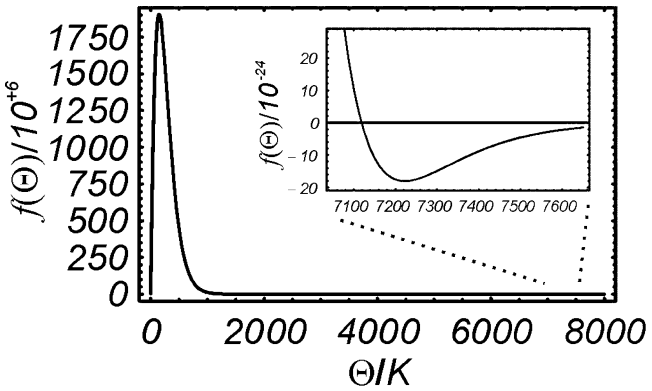

Figure 1. Graph of $f(\Theta)$. The finite, nonzero root at $\Theta = 7120$K minimizes the weighted sum of squared residuals $\xi(a,b,\Theta)$ (eq 13) and leads to $\Delta H = R\Theta = 14.1$kcal/mol.

variations in the best-fit enthalpy and entropy of $\mp$ 1 kcal/mol and $\mp$ 10 cal/mol K, respectively, are observed in fits to transition state theory.[19] Bain and co-workers[25] have similarly noted for Eyring plots that the first few low-temperature data points can skew the best-fit entropy and lead to substantial systematic errors. As errors in $1/T_2$ show up as nonlinearity in the Eyring plot, one can judge the quality of this choice based on the linearity of the plot. In our earlier work with pyridine carboxamides,[19] we reported a method for treating rate data that suppresses the sensitivity of the fit parameters to errors in the slow exchange T_2 by fitting the derivative of the rate versus temperature. This method is effective, but, as it uses finite differences, it is subject to increased random errors.

In this work, we account for transverse relaxation by fitting the half-width r to the functional form

$$r(T;a,b,\Theta) = b + aTe^{-\Theta/T} \tag{12}$$

Comparing eq 12 to eq 5 and to the rate expression (eq 11) from transition state theory, we identify the fit parameter Θ with $\Delta H^{\ddagger}/R$, a with $(k_B/h)e^{+\Delta S^{\ddagger}/R}$, and b with $1/T_2$. Parameter estimation could be done by nonlinear least-squares fitting to this three-parameter model. The model, a temperature-weighted exponential plus a constant, is closely related to the problem of fitting two exponentials, which is known to converge poorly. Indeed, for our data, standard nonlinear least-squares procedures (in *Mathematica*) reported Θ's that differed by nearly 10% from the global χ^2 minimum without signaling error. Fortunately, two of the parameters, a and b, enter linearly into eq 12, and so we adapt a method described by Jeričević et al., which converts the fitting procedure, a fine search of a three-dimensional parameter space that may contain local minima, to what is essentially the solution of a one-variable transcendental equation.[23] This method rapidly yields best-fit parameters guaranteed to be globally optimal.[23]

In this approach, the merit function to be minimized is a weighted sum of squared residuals

$$\xi(a,b,\Theta) = \sum_{i=1}^{n} w_i(r_i - r(T_i;a,b,\Theta))^2 \tag{13}$$

where n is the number of data points, and where the r_i, T_i, and w_i are the half-width, temperature, and weight of data point i. We obtain optimal parameters a, b, and Θ by setting the partial derivatives of ξ to zero. Three equations are obtained. These equations are linear in the parameters a and b and can be written in matrix form:

$$\begin{pmatrix} \sum w_iT_i^2e^{-2\Theta/T_i} & \sum w_iT_ie^{-\Theta/T_i} & -\sum w_iy_iT_ie^{-\Theta/T_i} \\ \sum w_iT_ie^{-\Theta/T_i} & \sum w_i & -\sum w_iy_i \\ \sum w_iT_ie^{-2\Theta/T_i} & \sum w_ie^{-\Theta/T_i} & -\sum w_iy_ie^{-\Theta/T_i} \end{pmatrix} \begin{pmatrix} a \\ b \\ 1 \end{pmatrix} = \begin{pmatrix} 0 \\ 0 \\ 0 \end{pmatrix} \tag{14}$$

The linearity of eq 14 with respect to a and b is crucial. The three equations can be solved (pairwise) for a and b, with the resulting expressions substituted into the remaining equation. The result is a single transcendental equation for Θ, which is readily solved numerically on a computer. Note that the matrix depends only on Θ and on the data. In order for the left-hand side to be zero, the determinant of the matrix must vanish. This determinantal equation

$$f(\Theta) = Det(\mathbf{F}) = 0 \tag{15}$$

where $\mathbf{F}$ is the matrix appearing in eq 14, is precisely the transcendental equation for the parameter Θ that is obtained by substitution to eliminate a and b.

Figure 1 shows a plot of $f(\Theta)$ for typical values of the data. There are three roots of $f(\Theta)$ evident, two of which ($\Theta = 0$ and $\Theta \rightarrow \infty$) are pathological because they essentially remove the exponential from the model function. The third root gives the optimal value of the parameter Θ, from which we obtain $\Delta H^{\ddagger} = R\Theta$. This solution can subsequently be used to construct the sums in the matrix $\mathbf{F}$. If we again solve equations pairwise from eq 14, then we may write three independent equations each for the a and b parameters:

$$a = \frac{\sum w_iT_ie^{-\Theta/T_i} \sum w_iy_i - \sum w_i \sum w_iy_iT_ie^{-\Theta/T_i}}{(\sum w_iT_ie^{-\Theta/T_i})^2 - \sum w_i \sum w_iT_i^2e^{-2\Theta/T_i}} \tag{16a}$$

or

$$\frac{\sum w_iT_ie^{-\Theta/T_i} \sum w_iy_ie^{-\Theta/T_i} - \sum w_ie^{-\Theta/T_i} \sum w_iy_iT_ie^{-\Theta/T_i}}{\sum w_iT_ie^{-\Theta/T_i} \sum w_iT_ie^{-2\Theta/T_i} - \sum w_ie^{-\Theta/T_i} \sum w_iT_i^2e^{-2\Theta/T_i}} \tag{16b}$$

or

$$\frac{\sum w_ie^{-\Theta/T_i} \sum w_iy_i - \sum w_i \sum w_iy_ie^{-\Theta/T_i}}{\sum w_iT_ie^{-\Theta/T_i} \sum w_ie^{-\Theta/T_i} - \sum w_i \sum w_iT_ie^{-2\Theta/T_i}} \tag{16c}$$

and

$$b = \frac{\sum w_iT_ie^{-\Theta/T_i} \sum w_iy_iT_ie^{-\Theta/T_i} - \sum w_iy_i \sum w_iT_i^2e^{-2\Theta/T_i}}{(\sum w_iT_ie^{-\Theta/T_i})^2 - \sum w_i \sum w_iT_i^2e^{-2\Theta/T_i}} \tag{17a}$$

or

$$\frac{\sum w_iT_ie^{-2\Theta/T_i} \sum w_iy_iT_ie^{-\Theta/T_i} - \sum w_iy_ie^{-\Theta/T_i} \sum w_iT_i^2e^{-2\Theta/T_i}}{\sum w_iT_ie^{-\Theta/T_i} \sum w_iT_ie^{-2\Theta/T_i} - \sum w_ie^{-\Theta/T_i} \sum w_iT_i^2e^{-2\Theta/T_i}} \tag{17b}$$

or

$$\frac{\sum w_iT_ie^{-\Theta/T_i} \sum w_iy_ie^{-\Theta/T_i} - \sum w_iy_i \sum w_iT_ie^{-2\Theta/T_i}}{\sum w_iT_ie^{-\Theta/T_i} \sum w_ie^{-\Theta/T_i} - \sum w_i \sum w_iT_ie^{-2\Theta/T_i}} \tag{17c}$$

depending on which pair is chosen. The best-fit solution for Θ obtained by solving eq 15 is the unique value that makes all of these expressions consistent. From this calculated value of a, we may compute $\Delta S^{\ddagger} = R \ln(ha/k_B)$ and from b obtain the average $1/T_2$ over the temperature range. The key insight is that the model function $r(T;a,b,\Theta)$ depends nonlinearly on only one of the parameters, Θ. Linearity with respect to a and b allows the transformations that provide a globally optimal fit to the rate data without a time-intensive fine search of a three-dimensional parameter space.

Experiment

^{1}H NMR spectra were recorded on a Varian Inova spectrometer (^{1}H frequency 300 MHz) equipped with a 5 mm high-resolution probe. Spectra were acquired over a range of temperatures from 0 °C to 60 °C (273 K to 333 K) using an FTS Systems AIRJET temperature preconditioner. Samples of isonicotinamide (Aldrich) were prepared in deuterated nitrobenzene (Cambridge Isotope Laboratories) at 5 mg/mL and placed in the inner portion of a 5/3 mm (OD) double NMR tube (Wilmad Glass). The outer tube was filled with ethylene glycol (Aldrich) for temperature calibration.[28] A rough estimate of the temperature was provided by the probe thermocouple while the actual temperature was determined using the chemical shift of ethylene glycol in thermal contact with the sample. This method was found to provide the most accurate temperature reading for the sample.

A one-pulse experiment with CYCLOPS phase cycling[29] was used to obtain the NMR data. Apparent rates were extracted from the real parts of the measured spectra using a nonlinear least-squares fitting program written within the *Mathematica* programming environment.[30] In addition to the resonance line positions $\sigma \pm \epsilon$, peak amplitude A, half-width r, and exchange-induced phase lean $\tan^{-1}(k/\epsilon)$, our fitting model included an overall phase correction and a cubic baseline correction. Whenever possible, nonexchanging peaks were excluded from the region of the spectrum that was fit. In the cases of spectral overlap with nonexchanging peaks, additional Lorentzian lines were incorporated into the model to accommodate these resonances.

The extracted half-widths were used as apparent rates in eqs 15−17 to estimate both the entropy and enthalpy of activation associated with the barrier to amide bond rotation according to transition state theory.[24,27] This procedure was again performed in *Mathematica*, with the data weighted inversely proportional to numerically estimated variances of the measured half-widths. The variances of the half-widths were roughly proportional to the half-widths themselves. The result of the linearized fitting procedure described in the previous section was a composite curve consisting of a constant plus the temperature-weighted exponential rise of transition-state theory. Uncertainties in $\Delta H^{\ddagger}$ and $\Delta S^{\ddagger}$ were determined through numerical calculation of the covariance matrix and are reported as ± one standard error.[31]

Ab initio calculations were performed at the restricted Hartree−Fock, MP2 electron correlation, and density functional (DFT) levels of theory using the Gaussian 98 software package.[32] For each level of theory, molecules were optimized without constraint to their ground and transition state geometries using the 6-31G(d,p) basis[33] with corresponding single-point energies calculated with the 6-311++G(d,p) basis. Ground and transition states were verified by frequency analysis after optimization, and zero-point energy corrections were applied with the appropriate scaling.[34,35] For density functional calculations, the B3LYP functional was chosen.[36−38]

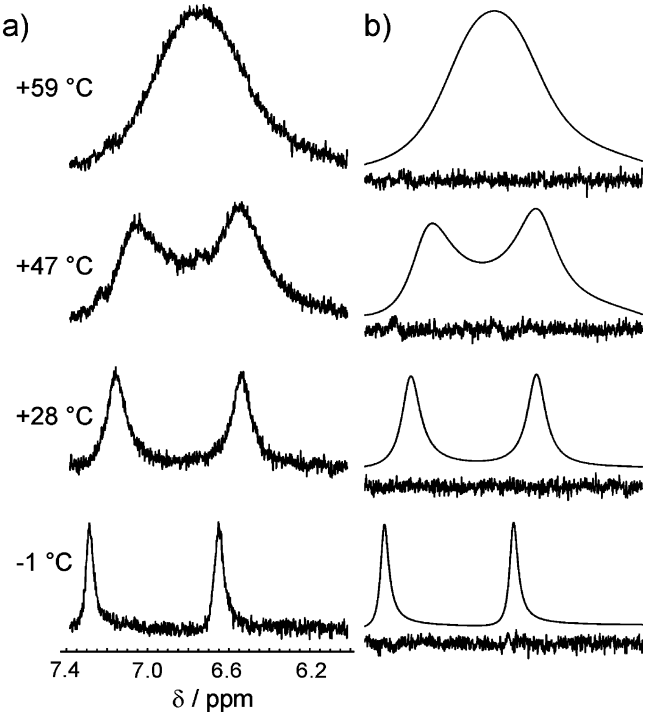

Figure 2. Dynamic NMR spectra of isonicotinamide over a 60 °C range of temperature. (a) Only the spectral region of the amide protons is shown. Under chemical exchange, the spectral lines broaden and then coalesce into a single peak. In this regime, the line shapes are a sensitive function of the exchange rate. (b) Results of the fitting procedure, including residuals from the fits. Note that small errors in overall phase are easily incorporated into the fitting model.

Results and Discussion

Figure 2a shows spectra of isonicotinamide at several different temperatures, each characterized by a different rate of exchange. At lower temperatures, separate resonances are observed for the chemically distinct amide protons. As the temperature rises and the exchange rate increases, the lines initially broaden and then coalesce ($T = 59$ °C $= 332$ K) into a single peak that sharpens as the temperature is further increased. Figure 2b shows fits to the two-site exchange model and fit residuals for the spectra shown in Figure 2a. The extracted apparent rates as a function of temperature are summarized in Table 1 and shown graphically in Figure 3a. Figure 3a also includes a best-fit curve of the form

$$r = \frac{1}{T_2} + \frac{k_B T}{h} e^{+\Delta S^{\ddagger}/R} e^{-\Delta H^{\ddagger}/RT} \qquad (18)$$

which restates eq 12 in terms of $\Delta H^{\ddagger}$, $\Delta S^{\ddagger}$, and T_2 rather than Θ, a, and b. The best-fit values $\Delta H^{\ddagger} = +14.1 \pm 0.2$ kcal/mol, $\Delta S^{\ddagger} = -5.2 \pm 1.2$ cal/mol K, and $T_2 = 46.7 \pm 1.5$ ms ($\Delta\nu = 6.81$ Hz) characterize the curve.

The estimated uncertainties, which are ± one standard error, are diagonal elements of the formal covariance matrix. The (off-diagonal) covariances are also of interest. In particular, we find that errors in the best-fit entropy and enthalpy are correlated in a way that makes $\Delta G^{\ddagger} = \Delta H^{\ddagger} - T\Delta S^{\ddagger}$ relatively insensitive to errors. As expected, the correlation coefficients involving T_2 are large (0.83 and 0.82, respectively, for correlation to $\Delta H^{\ddagger}$ and $\Delta S^{\ddagger}$). This strong correlation between errors in T_2 and errors in best-fit estimates of both $\Delta H^{\ddagger}$ and $\Delta S^{\ddagger}$ has also been noted by Bain and co-workers.[25] Such high correlation coefficients motivate our interest in retaining T_2 as a fit parameter over the observed temperature range.

TABLE 1: Experimental Data Points for Isonicotinamide in Nitrobenzene

T (K)	apparent rate (s^{-1})	*T* (K)	apparent rate (s^{-1})
272.3	22.58	298.5	39.67
273.3	23.12	299.6	46.46
274.0	23.67	300.3	46.74
274.9	23.48	300.8	50.66
276.6	24.65	301.8	50.93
277.7	24.39	302.6	49.20
278.7	24.88	303.5	52.63
279.7	25.36	304.5	54.60
280.4	24.67	305.6	58.95
281.0	27.02	306.5	61.63
282.0	26.55	307.4	65.33
283.1	28.23	308.4	66.87
284.2	28.82	309.3	68.08
285.1	28.60	310.7	74.23
286.1	28.78	311.4	77.72
286.9	28.93	312.0	81.67
287.8	28.37	313.0	86.37
288.8	28.40	314.1	86.14
289.8	28.77	315.5	91.38
290.6	30.19	316.1	98.25
291.2	30.94	317.0	102.9
292.2	31.20	318.1	107.8
293.3	34.50	319.0	117.1
294.6	35.06	319.8	116.6
295.4	35.16	320.7	121.1
296.3	36.93	321.5	142.9
297.2	37.57	322.7	153.0
297.7	39.53		

For comparison, we also show the rate data in terms of an Eyring plot (of ln k/T vs. $1/T$) in Figure 3b. The rates used in this plot are the result of subtracting the best-fit $1/T_2$ (from the fit described above) from the raw apparent-rate data. A linear least-squares fit to this plot yields $\Delta H^{\ddagger} = +14.2$ kcal/mol and $\Delta S^{\ddagger} = -5.0$ cal/mol K, and these values characterize the line shown. The close agreement between these values and those obtained from the linearized fitting procedure is likely the result of having put in the best-fit value of $1/T_2$ a priori. Indeed, varying this a priori "intrinsic width" by 5% causes a change in the extracted $\Delta H^{\ddagger}$ of 1.4 kcal/mol with no visible "curving" of the Eyring plot.

Comparison to Isomers and ab Initio Results. The enthalpy of activation for isonicotinamide, $+14.1 \pm 0.2$ kcal/mol, is between the values for nicotinamide, $+13.1 \pm 0.3$ kcal/mol, and picolinamide, $+17.9 \pm 0.4$ kcal/mol, reported in an earlier study.[19] Ab initio calculations detailed in that study were useful in quantitatively partitioning the barrier energies in nicotinamide and picolinamide into contributions from steric, hydrogen-bonding, and electronic effects. In particular, nicotinamide's ground state is characterized by a steric interaction between an amide proton and a proton on the pyridine ring, which leads to partial pyramidalization of the amide nitrogen and which lowers the barrier to rotation relative to picolinamide's. Picolinamide does not suffer from this steric interaction because the ring nitrogen is disposed ortho to the carboxamide moiety (Scheme 1). This ortho relationship also gives rise to a hydrogen bond in picolinamide between the amide proton and the pyridine nitrogen in the ground state, which contributes significantly to picolinamide's higher barrier.

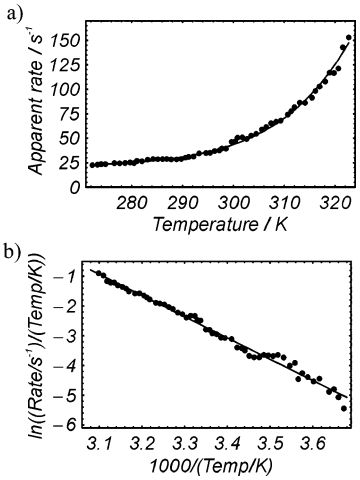

Figure 3. Apparent-rate data fit to transition state theory. (a) The temperature dependence of the apparent rate shown as a nonlinear fit. (b) Eyring plot.

These two effects alone were insufficient fully to account for the difference in the barriers. π-electron donation from the pyridine ring to the carbonyl carbon tends to stabilize lone-pair electron density on the amide nitrogen, and this electronic effect reduces the energy of the transition state for amide bond rotation. Scheme 2 shows rotational pathways for the pyridine carboxamides, including the roughly planar ground state and two transition states, in which the amide nitrogen is pyramidalized and the amide protons are disposed above and below the plane of the page. The reduction in energy of the transition state due to π-electron donation is most pronounced when the pyridine nitrogen is disposed in the position meta to the carboxamide as it is in nicotinamide. The resonance structures[39] shown in Scheme 3 illustrate how the position of the relatively electronegative nitrogen affects π-electron donation. In the roughly planar ground states of both picolinamide and nicotinamide (and in isonicotinamide), all three resonance structures shown are important, but I and II dominate. In the transition state, where the hydrogens are out of the plane defined by the ring atoms, structure I is no longer relevant, and the importance of structure III increases. In this resonance structure, positive charge is distributed by resonance over three carbons in nicotinamide, while in picolinamide it is distributed over two carbons and a more electronegative nitrogen atom. Because of this less favorable delocalization, picolinamide's transition state is stabilized by resonance to a lesser degree than nicotinamide's.

SCHEME 2: Rotational Pathways for Pyridine Carboxamides (Nicotinamide shown. I,N,P denote position of nitrogen atom in isonicotinamide, nicotinamide, and picolinamide)

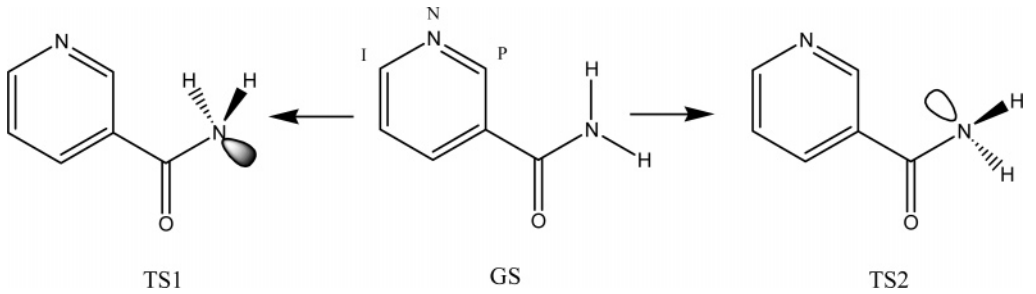

SCHEME 3: Resonance Structures for Picolinamide (top), Nicotinamide (middle), and Isonicotinamide (bottom)

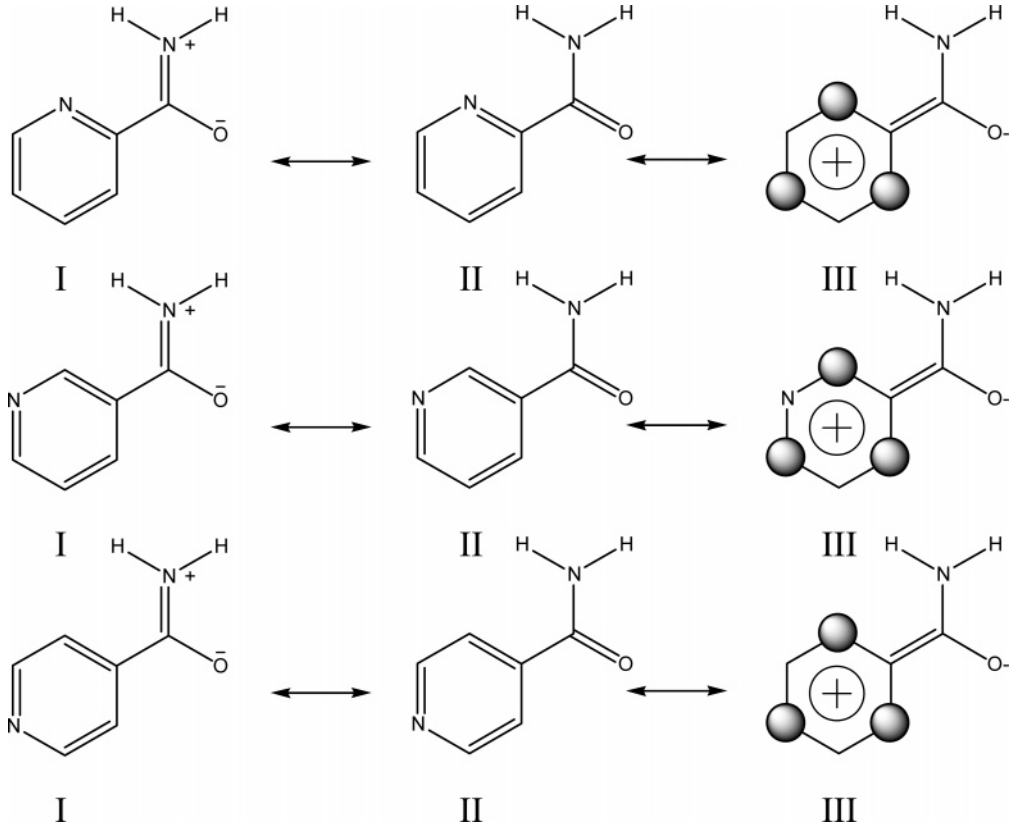

TABLE 2: Optimized Molecular Parameters[a]

	dihedral angle[c] N−C−C−C	nitrogen pyramidalization angle[c]	dipole moment[b]	C−N bond[d]	N−H1 bond[d]	N−H2 bond[d]
nicotinamide						
ground state	19.8	354.0	2.13	1.358	0.992	0.995
transition state	0.0	320.6	0.47	1.433	1.005	1.005
isonicotinamide						
ground state	24.7	354.3	3.56	1.357	0.993	0.995
transition state	0.0	321.6	2.29	1.429	1.004	1.004

[a] Structures optimized at HF/6-31G(d,p). [b] Dipole moment in Debye. [c] Angle in degrees. [d] Bond length in angstroms.

This leads to a 1−2 kcal/mol contribution to the difference in the barriers to rotation in nicotinamide and picolinamide.[19]

In isonicotinamide the pyridine nitrogen is para to the carboxamide moiety, and the same resonance considerations apply. Positive charge is distributed over two carbons and a more electronegative nitrogen, destabilizing the transition state relative to nicotinamide's. Since steric interactions in the ground states of nicotinamide and isonicotinamide are nearly the same, and since intramolecular hydrogen bonding is absent in both molecules, the difference in rotational barriers in these molecules, 1.0 kcal/mol, is likely dominated by this differential π-electron donation.

Figure 4 shows the results of ab initio calculations for nicotinamide and isonicotinamide in both their ground and transition states. Picolinamide is also shown. As is typical of amides, the ground states exhibit a roughly planar geometry for the amide nitrogen. The planar geometry allows for delocalization of π electrons between the amide nitrogen and the carbonyl carbon. Steric interactions with the pyridine ring protons impose slight (but roughly equivalent) deviations from planarity at the amide nitrogen and a twist of the N−C−C plane relative to the pyridine-ring plane in the ground states of both nicotinamide and isonicotinamide. This twist is slightly more pronounced for isonicotinamide (by 5°) and essentially absent

Figure 4. Molecular structures of nicotinamide, isonicotinamide, and picolinamide as determined by ab initio calculation. Both ground and transition states are shown.

in picolinamide. The transition states for nicotinamide and isonicotinamide are very similar in structure, with the nitrogens pyramidalized to the same degree and the protons pointing away from the ring as suggested by TS2 of Scheme 2, again likely due to steric interactions. Table 2 details the geometric data quantitatively for nicotinamide and isonicotinamide.

The ab initio energies characterizing the gas phase rotational barriers are detailed in Table 3. The experimentally determined activation enthalpies for nicotinamide and isonicotinamide agree

TABLE 3: Amide Rotational Barrier of Pyridine Carboxamides (in kcal/mol)

	rotational barrier (TS1)	rotational barrier (TS2)
isonicotinamide		
HF/6-311++G(d,p)[a]	17.3	12.7
B3LYP/6-311++G(d,p)[b]	18.5	14.1
MP2/6-311++G(d,p)[a]	17.5	13.1
measured	14.1	
nicotinamide		
HF/6-311++G(d,p)[a]	16.2	11.5
B3LYP/6-311++G(d,p)[b]	17.4	13.2
MP2/6-311++G(d,p)[a]	16.4	12.5
measured	13.1	
picolinamide		
HF/6-311++G(d,p)[a]	18.4	20.4
B3LYP/6-311++G(d,p)[b]	20.1	22.2
MP2/6-311++G(d,p)[a]	18.2	20.5
measured	17.9	

[a] Structure minimized at HF/6-31G(d,p). Corrected with zero point energies at HF/6-31G(d,p) scaled by 0.9. [b] Structure minimized at B3LYP/6-31G(d,p). Corrected with zero point energies at B3LYP/6-31G(d,p) scaled by 0.96.

to within 0.1 kcal/mol with the lower energetic barriers calculated with density functional theory. The Hartree−Fock and MP2 calculations for all barriers are 1−2 kcal/mol lower than those for DFT. The agreement with experiment is good even though no account is taken of solvent interactions in the calculations. The likely similarity of solvent interactions with nicotinamide and isonicotinamide in any case strengthens our primary conclusion that the 1.0 kcal/mol greater barrier in isonicotinamide is indeed likely dominated by less favorable delocalization of positive charge over the pyridine ring in the transition state.

Concluding Remarks

This work details measurements of the amide rotational barrier in isonicotinamide from dynamic NMR data and comparisons to previously reported barriers of regioisomers. A fitting procedure that incorporates transverse relaxation over the whole slow-exchange temperature range is used to mitigate errors caused by extrapolation of a "limiting line width" solely from slow-exchange data. As the fitting model is nonlinear in only one of the fit parameters (the activation enthalpy), parameter estimation is reduced to solution of a single transcendental equation, avoiding a fine search over a multidimensional parameter space that can be more susceptible to numerical errors. This procedure is amenable to extension to more complicated models for temperature-dependent transverse relaxation. For example, one could incorporate a temperature-dependent $1/T_2$ with constant and linear terms by modeling the apparent rate with the function

$$r(T;a,b,c,\Theta) = b + cT + aTe^{-\Theta/T} \qquad (19)$$

while still retaining the key advantage of the procedure, that only solution of a single transcendental equation is necessary to extract kinetic parameters.

The activation enthalpy measured for isonicotinamide, $\Delta H^{\ddagger} = +14.1 \pm 0.2$ kcal/mol, falls between those of its regioisomers picolinamide and nicotinamide. The experimentally determined activation enthalpies agree to within 0.1 kcal/mol with energetic barriers calculated with density functional theory. A direct comparison between isonicotinamide and nicotinamide, where steric and hydrogen-bonding effects differ only slightly, yields a more quantitative picture of the effect of π-electron donation from the pyridine ring to the carboxamide in these biochemically significant molecules.

Acknowledgment. This work was supported in part by NSF grants CHE-0349345 and CCF-0432186 to L.J.M. and NIH Grant 1R15 GM061584-01 and Luce Foundation funding to M.E.H. R.A.O. is a Department of Education GAANN Fellow.

References and Notes

(1) Taha, A.; True, N. *J. Phys. Chem. A* **2000**, *104*, 2985.
(2) Stewart, W. E.; Siddall, T. H. *Chem. Rev.* **1970**, *70*, 517.
(3) Rabinovitz, M.; Pines, A. *J. Am. Chem. Soc.* **1969**, *91*, 1585.
(4) Bain, A. D.; Hazendonk, P.; Couture, P. *Can. J. Chem.* **1999**, *77*, 1340.
(5) Fontoura, L. A. M.; da Cruz Rigotti, I. J.; Correia, C. R. D. *J. Mol. Struct.* **2002**, *609*, 73.
(6) Wiberg, K. B.; Laidig, K. E. *J. Am. Chem. Soc.* **1987**, *109*, 5935.
(7) Wiberg, K. B.; Breneman, C. M. *J. Am. Chem. Soc.* **1992**, *114*, 831.
(8) Wiberg, K. B.; Hadad, C. M.; Rablen, P. R.; Cioslowski, J. J. *J. Am. Chem. Soc.* **1992**, *114*, 8644.
(9) Wiberg, K. B.; Rablen, P. R.; Rush, D. J.; Keith, T. A. *J. Am. Chem. Soc.* **1995**, *117*, 4261.
(10) Fogarasi, G.; Szalay, P. G. *J. Phys. Chem. A* **1997**, *101*, 1400.
(11) Basch, H.; Shmaryahu, H. *Chem. Phys. Lett.* **1998**, *294*, 117.
(12) Bennet, A. J.; Wang, Q. P.; Slebocka-Tilk, H.; Somayaji, R. S.; Brown, R. S.; Santarsiero, B. D. *J. Am. Chem. Soc.* **1990**, *112*, 6383.
(13) Fisher, G. *Chem. Soc. Rev.* **2000**, *29*, 119.
(14) Campomanes, P.; Menendez, M. I.; Sordo, T. L. *J. Phys. Chem. A* **2002**, *106*, 2623.
(15) Cox, C.; Lectka, T. *J. Org. Chem.* **1998**, *63*, 2426.
(16) Berg, U.; Astrom, N. *Acta Chem. Scand.* **1995**, *49*, 599.
(17) Avalos, J. L.; Boeke, J. D.; Wolberger, C. *Mol. Cell* **2004**, *13*, 639.
(18) Smith, B. D.; Goodenough-Lashua, D. M.; D'Souza, C. J. E.; Norton, K. J.; Schmidt, L. M.; Tung, J. C. *Tetrahedron Lett.* **2004**, *45*, 2747.
(19) Olsen, R. A.; Liu, L.; Ghaderi, N.; Johns, A.; Hatcher, M. E.; Mueller, L. J. *J. Am. Chem. Soc.* **2003**, *125*, 10125.
(20) Sandstrom, J. *Dynamic NMR Spectroscopy*; Academic Press: London, 1982.
(21) Szymanski, S.; Witanowski, M.; Gryff-Keller, A. *Ann. Rep. NMR Spectrosc.* **1978**, *8*, 227.
(22) Drakenberg, T.; Carter, R. E. *Org. Mag. Res.* **1975**, *7*, 307.
(23) (a) Jeričević, Z.; Benson, D. M.; Bryan, J.; Smith, L. C. *Anal. Chem.* **1987**, *59*, 658. (b) Gampp, H.; Maeder, M.; Zuberbuhler, A. D. *Anal. Chem.* **1988**, *60*, 1084.
(24) Bain, A. D. *Prog. NMR Spectrosc.* **2003**, *43*, 63.
(25) Bain, A. D.; Duns, G. J.; Ternieden, S.; Ma, J.; Werstiuk, N. H. *J. Phys. Chem.* **1994**, *98*, 7458.
(26) Binsch, G. *J. Am. Chem. Soc.* **1969**, *91*, 1304.
(27) Pechukas, P. *Annu. Rev. Phys. Chem.* **1981**, *32*, 159.
(28) Raiford, D. S.; Fisk, C. L.; Becker, E. D. *Anal. Chem.* **1979**, *51*, 2050.
(29) Hoult, D. I.; Richards, R. E. *Proc. R. Soc. (Lond)* **1975**, *A344*, 311.
(30) Wolfram, S. *Mathematica: A System for Doing Mathematics by Computer*; 2 ed.; Addison-Wesley Publishing Company: Reading, Massachusetts, 1991.
(31) Press, W. H.; Teukolsky, S. A.; Vetterling, W. T.; Flannery, B. P. *Numerical Recipes in C: the Art of Scientific Computing*, 2nd ed.; Cambridge University Press: Cambridge, 1992.
(32) Frisch, M. J.; Trucks, G. W.; Schlegel, H. B.; Scuseria, G. E.; Robb, M. A.; Cheeseman, J. R.; Zakrzewski, V. G.; Montgomery, J. A., Jr.; Stratmann, R. E.; Burant, J. C.; Dapprich, S.; Millam, J. M.; Daniels, A. D.; Kudin, K. N.; Strain, M. C.; Farkas, O.; Tomasi, J.; Barone, V.; Cossi, M.; Cammi, R.; Mennucci, B.; Pomelli, C.; Adamo, C.; Clifford, S.; Ochterski, J.; Petersson, G. A.; Ayala, P. Y.; Cui, Q.; Morokuma, K.; Malick, D. K.; Rabuck, A. D.; Raghavachari, K.; Foresman, J. B.; Cioslowski, J.; Ortiz, J. V.; Baboul, A. G.; Stefanov, B. B.; Liu, G.; Liashenko, A.; Piskorz, P.; Komaromi, I.; Gomperts, R.; Martin, R. L.; Fox, D. J.; Keith, T. A.; Al-Laham, M. A.; Peng, C. Y.; Nanayakkara, A.; Challacombe, M.; Gill, P. M. W.; Johnson, B.; Chen, W.; Wong, M. W.; Andres, J. L.; Gonzalez, C.; Head-Gordon, M.; Replogle, E. S.; Pople, J. A. *Gaussian 98*; Revision A.9 ed.; Gaussian, Inc: Pittsburgh, PA, 1998.
(33) Hehre, W. J.; Radom, L.; Schleyer, P. v. R.; Pople, J. A. *Ab Initio Molecular Orbital Theory*; Wiley: New York, 1986.
(34) El-Azhary, A. A.; Suter, H. U. *J. Phys. Chem.* **1996**, *100*, 15056.
(35) Pople, J. A.; Schlegel, H. B.; Krishnan, R.; Defrees, D. J.; Binkley, J. S.; Frisch, M. J.; Whiteside, R. A.; Hout, R. F.; Hehre, W. *J. Int. J. Quantum Chem. Symp.* **1981**, *15*, 269.
(36) Becke, A. D. *Phys. Rev. A.* **1988**, *38*, 3098.
(37) Becke, A. D. *J. Chem. Phys.* **1993**, *98*, 5648.
(38) Lee, C.; Yang, W.; Parr, R. G. *Phys. Rev. B.* **1988**, *37*, 785.
(39) Kallies, B.; Kleinpeter, E.; Koch, A.; Mitzner, R. *J. Mol. Struct.* **1997**, *435*, 123.